Automated registration of multi-mode nondestructive evaluation data

Peter W. Spaeth*[a], Erik L. Frankforter[a], William C. Schneck[a], Matthew R. Webster[a], Matthew Godbold[b], Daniel F. Perey[a]
[a]Nondestructive Evaluation Sciences Branch, NASA Langley Research Center, Hampton, VA USA
[b]McNAIR Aerospace Center, University of South Carolina, Columbia, SC, USA

ABSTRACT

Registration techniques play a central role in applications of image processing to computer vision, medical imaging, and automatic target tracking. Feature-based techniques such as scale-invariant feature transform (SIFT) and speeded up robust features (SURF) are commonly used to register images derived from a single modality. However, SIFT and SURF struggle to register images from different modalities because the features tend to manifest rather differently and at sometimes very different length-scales. The most successful methods that have been developed to register multi-modal data use information-theoretic approaches. These methods play a key part in nondestructive evaluation scenarios where data that is collected by sensors of different modalities must be registered to be fused. In this paper, automated registration based on normalized mutual information is applied to align data derived from ultrasonic and radiographic inspections of (i) additively manufactured titanium alloy test coupons, and (ii) thin, lithium metal pouch-cell batteries. The quality of the registration is quantified in terms of computational resources and spatial accuracy. In the first case the X-ray computed tomography (XCT) data is captured on a region corresponding to a small subset of the ultrasonic data, while in the case of the lithium batteries the digital radiography (DR) captures a larger region of interest than the ultrasonic data. In both cases the radiographic data resolution is much higher than for ultrasound, but interestingly, in both cases the accuracy of the registration is approximately equal to two-to-three-pixel lengths in the ultrasonic images.

Keywords: Data registration, data fusion, mutual information-based registration, feature extraction, ultrasound, digital radiography, X-ray computed tomography

1. INTRODUCTION

It is common to apply multiple nondestructive evaluation (NDE) methods to characterize a given material or specimen. For example, XCT is often used to provide ground-truth data to compare against other forms of NDE such as ultrasonic testing (UT). However, alignment of multi-mode NDE data is a challenging problem due to the dissimilar scales and features that are derived from different inspection methods. In both the examples presented in this paper, the SIFT [1] and SURF [2] approaches, despite being robust to changes in scale, were unable to derive useable features for registration even when combined with an iterative approach like random sample consensus (RANSAC) [3] or iterative closest points (ICP) [4]. An additional challenge in computing features that is faced in this work arises from the relative uniformity of the foreground pixel intensities of the images.

An alternative approach that has been developed in biomedical imaging to align XCT and magnetic resonance (MR) data is to estimate the registration that maximizes the mutual information of the source and target data sets [5, 6]. A comprehensive review of information-based approaches to data registration is given in [7], which points out that, 'Registration of ultrasound images to other modalities using mutual information is a relatively unexplored field.' Previous studies [8, 9, 10] have explored the possibility of using mutual information for ultrasound-to-anatomical MR image registration. More recently, Dahman et al. [11] studied ultrasound-to-XCT registration using normalized mutual information; however, in that case the data are anatomical, and the ultrasound images are synthesized directly from the XCT data. The focus of this paper is to explore UT-to-DR and XCT-to-UT registration on non-synthesized NDE data.

The initial work in information-theoretic registration [5, 6] was based on maximizing the mutual information of the aligned images. However, spurious registrations can result when background pixel intensities dominate the calculation of mutual information at the expense of the foreground, as is the case in the images studied in this paper. Hence it is important to use an approach that is invariant to overlap statistics such as using normalized mutual information registration from Studholme et al. [12]. In this approach overlap invariance is achieved by computing the registration that minimizes the joint entropy with respect to the marginal entropies of the images.

*peter.w.spaeth@nasa.gov; phone 1 757 864-8622; fax 1 757 864-4914

2. METHODS

The essence of the normalized mutual information-based approach to image registration from [12] is to treat pixel intensities as random variables and find the transformation that minimizes the entropy of their overlap with respect to the marginal entropies. Using more precise terminology, the normalized mutual information of source and target images A and B is equal to

$$Y(A,B) = \frac{H(A) + H(B)}{H(A,B)} \tag{1}$$

where

$$H(X) = \sum_{x \in X} x \log \frac{1}{x} \tag{2}$$

is the log entropy of a random variable X.

In this paper normalized mutual information was used to align images in two different settings, but in both cases the registration is treated as a template matching problem where the source image or 'template' A is placed in a larger scene or 'target' image B, and the mapping from A into B is restricted to be a translation.

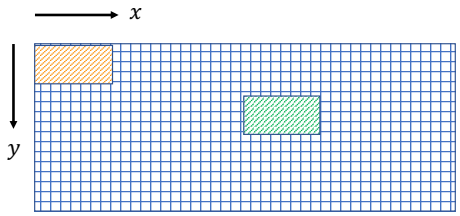

Figure 1. Template matching. Source image (shown in red) is translated to target location (green) within a larger scene (blue) by computing the translation that maximizes the mutual information content of the overlap between source and target.

Several methods are available for computing the translation that optimizes $Y(A,B)$. A natural choice is given by Powell's conjugate direction method [13] because of its efficiency (it requires no differentiation) and ease of implementation. The basic algorithm in two-dimensions begins as follows. Given an objective function $f(x,y)$, an initial condition $\vec{x}_0 = (x_0, y_0)$ and directions (i.e., unit vectors) $\vec{s}_1$, and $\vec{s}_2$, (i) find the extremum, $\vec{x}_1$, of f at $\vec{x}_0$ in the direction of $\vec{s}_1$, (ii) find the extremum, $\vec{x}_2$, of f starting at $\vec{x}_1$ in the direction $\vec{s}_2$, and (iii) define the new direction $\vec{s}_3 = \vec{x}_2 - \vec{x}_0/(||\vec{x}_2 - \vec{x}_0||)$. The process repeats starting with the point $\vec{x}_2$ and the direction vectors $\vec{s}_2$ and $\vec{s}_3$ until it fails to produce a significant change in the function f, if the denominator of the new direction vector approaches zero, or after a fixed number of iterations. Powell's method is quadratically convergent and converges after a finite number of iterations when the function f is a quadratic function of n-variables.

3. RESULTS

The methods of the previous section were applied in two scenarios: first, to register a 2D image slice from a volumetric XCT image to a full-field ultrasound image of a titanium alloy fatigue specimen; and second, to register an ultrasound image to a composite digital radiograph of a thin pouch-cell battery.

3.1 Additive Manufactured fatigue specimens

A set of additive manufacturing specimens prepared as part of a fatigue study [14] was used. These specimens were produced via laser powder bed fusion (PBF), and manufactured with laser scan speed and power expected to produce lack-of-fusion porosity, nominally pristine conditions, and keyhole porosity.

Full-field UT data on these specimens were acquired using an immersion scan pulse-echo technique, using a spherically focused 20 MHz, 0.25" diameter transducer. The lateral sides of the fatigue specimen were elevated on blocks so the top and bottom surfaces were in contact with water. The top surface of the specimen was placed at the as-manufactured focal plane of the transducer by adjusting the height to the point that maximized the front-wall reflection. A raster scan was then

performed over the specimen in 0.005" increments, and resulting waveforms were digitized by a 16-bit, 180 MS/s PCIe card. See Figure 2a for a conceptual sketch of the pulse-echo inspection at an individual (x, y)-location in the scan, and Figure 2b for a representative waveform obtained from the neck region of a fatigue specimen.

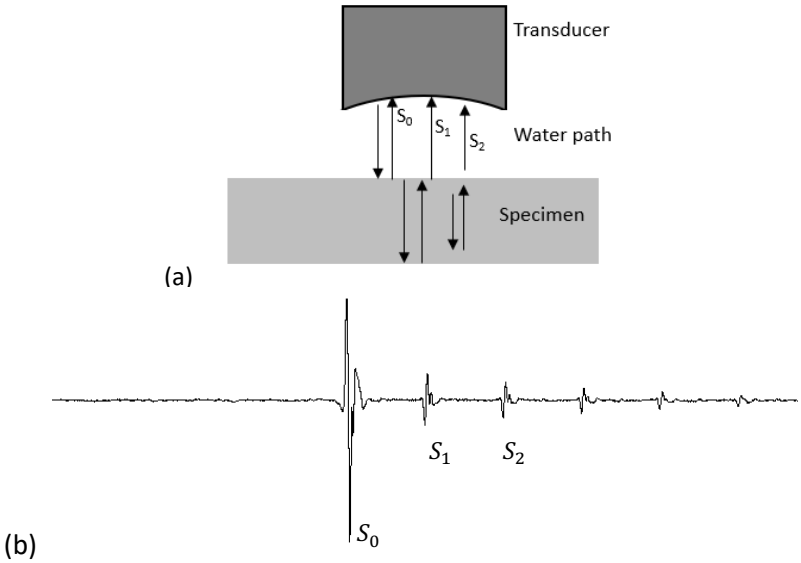

Figure 2. (a) Conceptual sketch of pulse-echo inspection with S0, S1, and S2 representing front-wall, back-wall, and second back-wall reflections, respectively. (b) Representative UT waveform obtained from central neck region of a fatigue specimen. (From [15])

UT data were obtained for one of the lack-of-fusion porosity specimens and used as a basis for the registration. The first back-wall reflection was assessed, as it contains information from the wave passing through the full thickness of the specimen and back (thus interacting with the porosity). The peak UT signal amplitude of the first back-wall reflection was found to exhibit a relatively high variance with discernable sections of low amplitude. For comparison, similar scans were performed on the nominally pristine specimens, which did not show the same high variance in signal amplitude for porosity conditions. For improved visualization of porosity, the first back-wall reflection was extracted, and a discrete Fourier transform (DFT) was applied to the waveforms at each (x, y)-location across the raster scan. The DFT was sliced at 21.3 MHz, and the resulting C-scan (Figure 3b) contains several large porosity indications in the specimen's central neck region.

In addition, XCT data centered on an approximately 8.5 mm central neck region were obtained at 5 µm voxel resolution. A two-dimensional slice of the reconstructed XCT (Figure 3) containing a large pore was identified for template matching with the larger UT region of interest so that the pore could be used for estimating error in the final alignment.

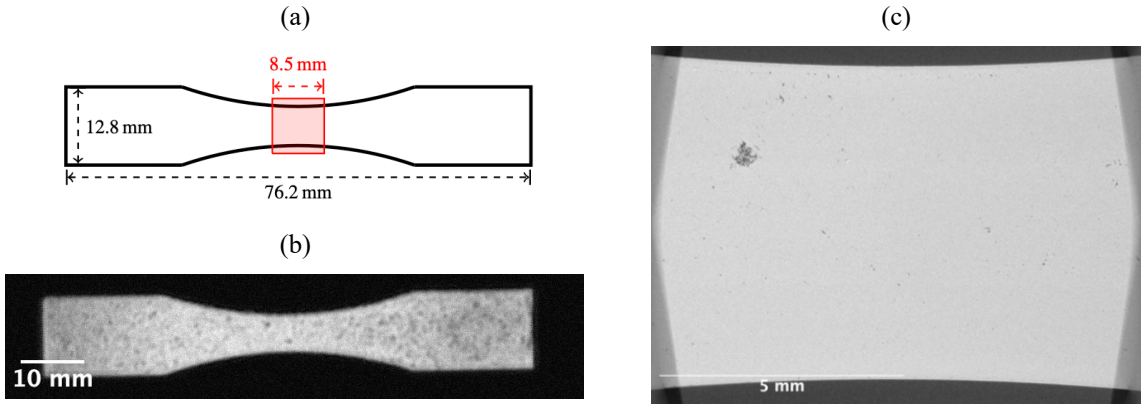

Figure 3. (a) Geometry of additively manufactured titanium alloy fatigue specimen showing in red the approximate location of XCT region of interest. (b) UT C-scan of the specimen. (c) XCT 2D-image slice containing a large pore. (Image source [15])

The XCT image is rescaled to match the pixel resolution of the UT image for template matching in the larger UT scene using Gaussian blur. The optimal translation is found by maximizing the mutual information content of the overlay using Powell's method (Figure 4).

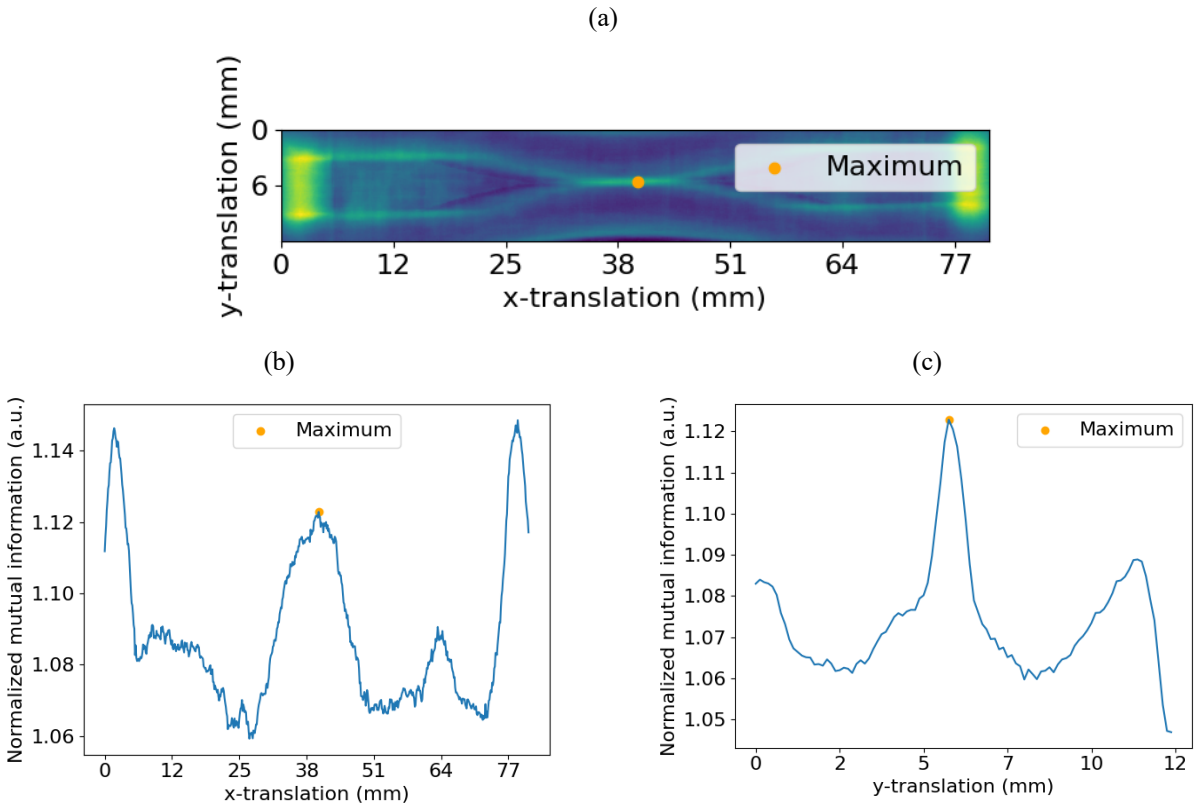

Figure 4. (a) Normalized mutual information as a function of the translation vector (x, y) for registering the titanium alloy fatigue specimen with the maximum value is shown in orange. Normalized mutual information as functions of x (b) and y (c) passing through the maximum identified by Powell's method in (a).

3.2 Lithium-metal cells

A 5"x4" lithium-metal pouch cell battery (Figure 5) was selected for multi-modal registration in this work. The cell consists of a single cathode-anode pair separated by a polymeric separator material. Two NDE techniques (UT and DR) were used to create images that were aligned using the template matching strategy outlined in Section 2.

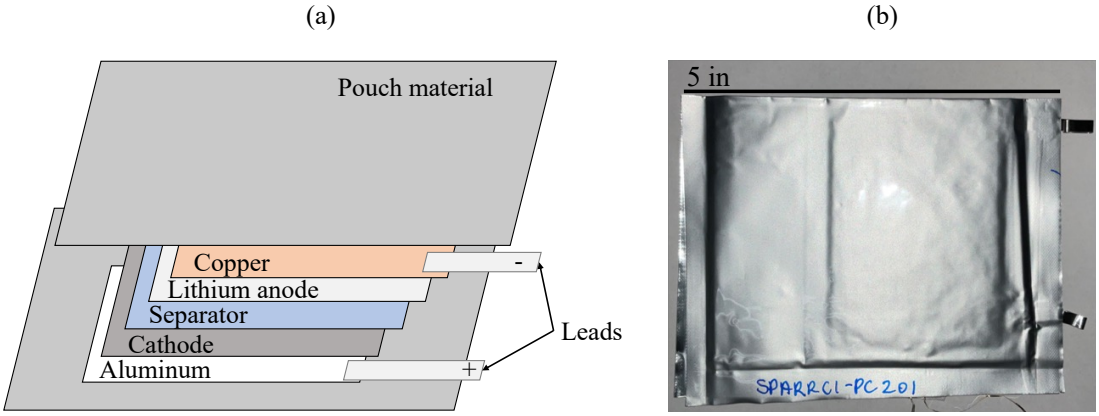

Figure 5. Lithium-metal pouch cell battery schematic (a) and digital image (b).

Digital Radiographs (DRs) were collected across the pouch cell (Figure 6a) at approximately 1500 pixel per inch resolution with a goal to identify dendritic structures in the lithium layer. Due to the make-up of the layers in the pouch cell an energy of 75kV was applied to capture the DRs. To image the entire battery, a raster scan of 12 images was stitched together to form a single composite image (Figure 6b).

(a) (b)

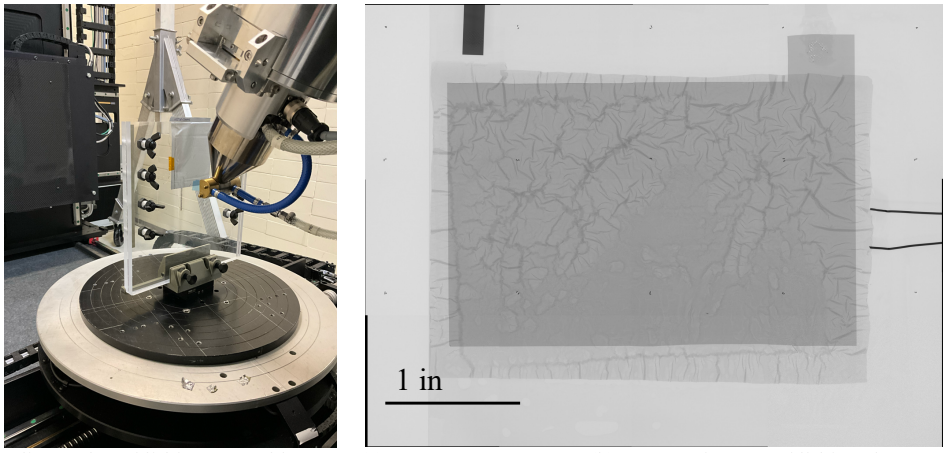

Figure 6. Digital radiography of lithium-metal battery. (a) X-ray system setup. (b) Composite DR of lithium battery at an approximate 10-micron pixel resolution.

Ultrasonic data was collected on the lithium metal pouch cell battery in pulse-echo mode using a nominally 10 MHz 0.5" diameter 2.0" focused ultrasonic transducer excited by a commercial pulser-receiver. The immersion transducer was used in a captured water column assembly (Figure 7a) in which the active face of the transducer was immersed in water, but a nitrile membrane separated the water in the column from the specimen under test. The nitrile membrane was coupled to the specimen through a light mist of water applied to the specimen surface, which made it possible to test the battery without fully submerging in water.

The captured water column was attached to a computer-controlled scanning gantry which scanned over a 3.2" x 2" region with a 0.01" step size in the x- and y-directions. Time domain data was collected at each scan point and the RMS amplitude of a select part of the signal was calculated. For this study the window analyzed had an approximate 1μs offset from the echo received from the battery surface (Figure 7b), as this type of delayed time gating has been found to improve contrast to the battery's internal structure [16]. The RMS amplitude at each scan point served as the pixel intensity in the c-scan images that were used for registration (Figure 7c).

(a) (b) (c)

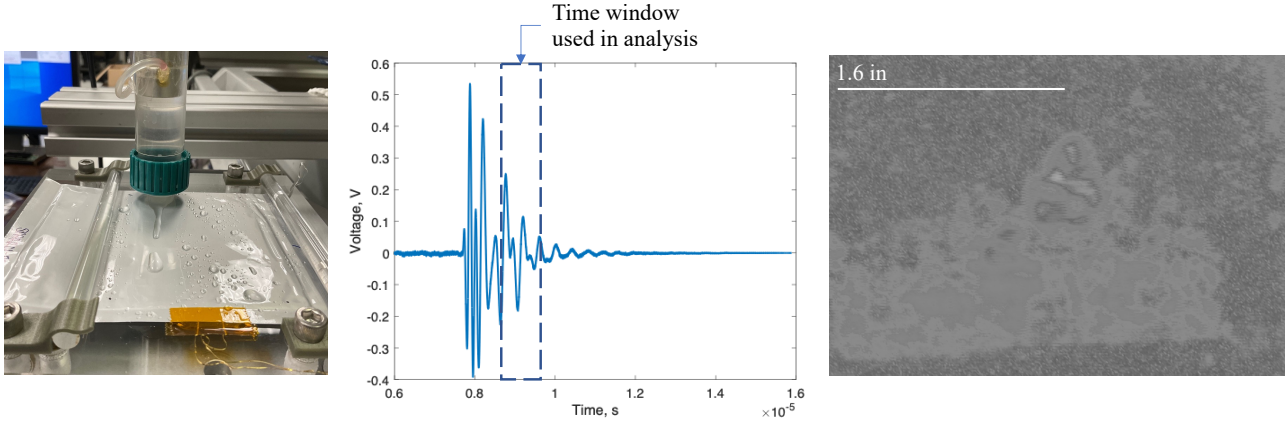

Figure 7. Images from ultrasonic testing of a lithium metal pouch cell battery. (a) Image of the testing apparatus showing the ultrasonic transducer in a captured water column. (b) Example data collected during ultrasonic testing showing the region analyzed for each inspection point on the battery surface. (c) Resulting ultrasound image.

The battery DR (Figure 6b) is first rescaled to match the pixel resolution of the UT image (Figure 7c) using Gaussian blur. The UT image is then treated as the tile to be placed in the larger scene defined by the down-sampled DR. The optimal translation was computed using Powell's algorithm and the results can be seen in (Figure 8).

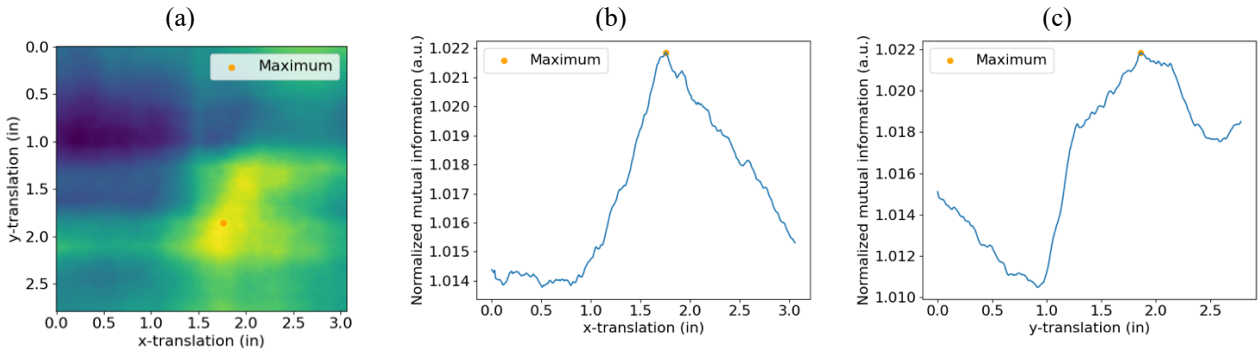

Figure 8. (a) Normalized mutual information as a function of the translation vector (x, y) for registering the lithium-metal pouch cell battery with the maximum value is shown in orange. Normalized mutual information as functions of x (b) and y (c) that passing through the maximum point identified by Powell's method in (a).

4. DISCUSSION

The accuracy of the registration was estimated manually by computing the distances between manually labelled key points in the registered images (Figure 9 and Figure 10). For the fatigue specimen the visible pore was selected for this purpose, while points along the boundary of a region with distinct texture that was visible in both the ultrasound and DR images were identified in the common coordinate system of the scenes.

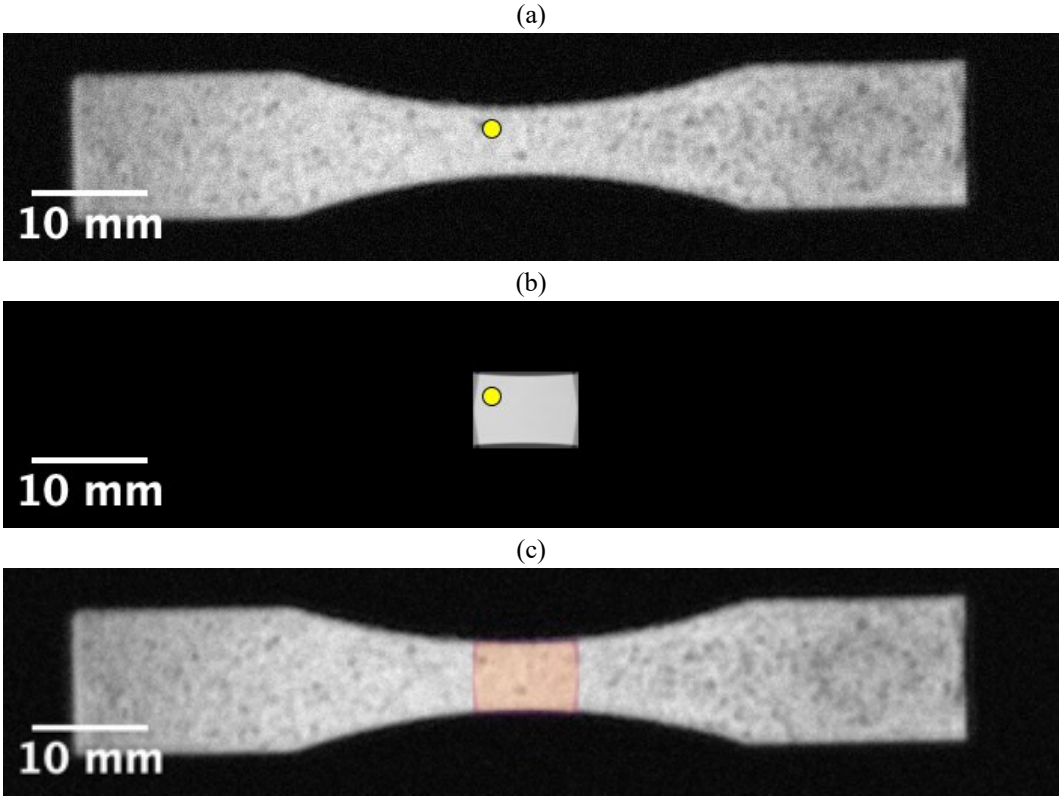

Figure 9. Registered UT (a) and XCT (b) images of the fatigue specimen. Manually labelled key points in the common coordinate system shown in yellow. (c) Overlayed images.

(d) (e) (f)

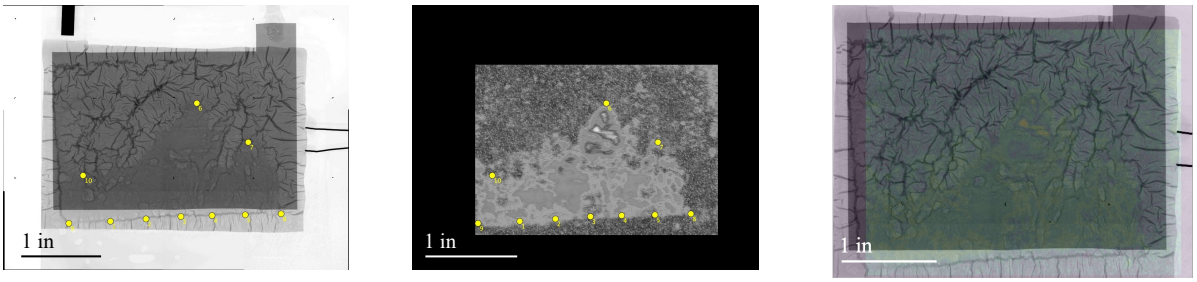

Figure 10. Registered UT (a) and XCT (b) images of the pouch cell battery. Manually labelled key points in the common coordinate system shown in yellow. (c) Overlayed images.

The error in the registration (Table 1) of the fatigue specimen was primarily due to an incorrect shift of approximately 2 pixels in the x direction while the error in the battery registration was due to a shift of approximately the same length in the y-direction.

Table 1. Accuracy of registration method for both the fatigue specimen and pouch cell battery.

	Ti-64Al-4V AM coupon	Li^+ battery
Estimated registration error	0.649 (mm)	0.648 (mm)

An empirical estimate (Table 2) of the time-complexity, N, of the implementation of the registration algorithm was estimated by comparing run-times of the battery registration problem for several rescalings of the source and target images against the running time and problem size of the registration of the fatigue specimen using the formula

$$N \log \frac{n_1}{n_2} = \log \frac{t_1}{t_2} \tag{3}$$

where n_1 and t_1 (respectively, n_2 and t_2) are the problem size (i.e., number of pixels) and run-time for battery registration (resp. fatigue specimen registration). The initial evidence suggests linear relationship between the running time as a function of the problem size.

Table 2. Empirical estimate of the time-complexity of registration algorithm.

	Computational time	Problem size	Time-complexity estimate N
Ti-64Al-4V AM coupon	0.59 (s)	101 pixels by 21 pixels	N/A
Li^+ battery	13.04 (s)	139 pixels by 153 pixels	1.29
Li^+ battery	74.19 (s)	307 pixels by 297 pixels	1.35
Li^+ battery	189.41 (s)	418 pixels by 469 pixels	1.28

5. CONCLUSIONS

In this paper the feasibility of using mutual information to register images derived from different NDE modalities was studied empirically for aligning ultrasound to digital radiography of thin lithium-metal pouch cell batteries and XCT to ultrasound images of titanium alloy fatigue specimens. In both cases the accuracy of the method was assessed using manually observed landmarks in the images and the approximate error was found to be approximately equal to two to three pixel-lengths in the respective ultrasound images. Moreover, the registration should enable the fusion of NDE data and future development of combined defect recognition methods for additively manufactured components and lithium-metal batteries. Improvements to the registration can likely be achieved by including gradients of the images with the pixel-

intensity based approach described in the paper. It will also be important to fully understand the computational time of the method as a function of problem size. Finally, generalizing the approach in this paper to rigid and projective registration will provide more flexibility in aligning multi-modal data registration.

REFERENCES

[1] D. Lowe, "Distinctive Image Features from Scale-Invariant Keypoints," *International Journal of Computer Vision,* vol. 50, no. 2, pp. 91-110, 2004.

[2] H. Bay, T. Tuytelaars and L. Gool, "Speeded-up robust features (SURF)," *Computer Vision and Image Understanding,* vol. 110, no. 3, pp. 346-359, 2008.

[3] M. Fischler and R. Bolles, "Random Sample Consensus: A Paradigm for Model Fitting with Applications to Image Analysis and Automated Cartography," *Comm. ACM,* vol. 24, no. 6, pp. 381-395, 1981.

[4] A. Somani, T. Huang and S. Blostein, "Least-square fitting of two 3-D point sets," *IEEE Pattern Analysis and Machine Intelligence,* vol. 9, no. 5, pp. 698-700, 1987.

[5] A. Collignon, F. Maes, D. Delaere, D. Vandermeulen, P. Suetens and G. Marchal, "Automated multimodality image registration using information theory," in *Information Processing in Medical Imaging*, Brest, Dordrecht, 1995.

[6] P. Viola and W. Wells, "Alignment by maximisation of mutual information," in *Proc. 5th Int. Conf. on Computer Vision*, Cambridge, MA, 1995.

[7] J. P. Pluim, "Mutual-Information-Based Registration of Medical Images: A Survey," *IEEE Transactions on Medical Imaging,* vol. 22, no. 8, pp. 986-1004, 2003.

[8] A. Roche, X. Pennec, G. Malandain and N. Ayache, "Rigid registration of 3-D ultrasound with MR images: A new approach combining intensity and gradient information," *IEEE Transactions of Medical Imaging,* vol. 20, no. 10, pp. 1038-1049, 2001.

[9] P. Slomka, J. Mandel, D. Downey and A. Fenster, "Evaluation of voxel-based registration of 3-D power Doppler ultrasound and 3-D magnetic resonance angiographic images of cardiod arteries," *Ultrasound Med. Biol.,* vol. 27, no. 7, pp. 945-955, 2001.

[10] J. Blackall, C. M. J. Rueckert, G. Penney, D. Hill and D. Hawkes, "An image registration approach to automated calibration for freehand 3D ultrasound," in *Medical Image Computing and Computer-Assisted Intervention*, Berlin, Springer-Verlag, 2000.

[11] B. Dahman, F. Bessière and J.-L. Dillenseger, "Ultrasound to CT rigid image registration using CNN for the HIFU treatment of heart arrhythmias," in *SPIE Medical Imaging*, San Diego, CA, 2022.

[12] C. Studholme, D. Hill and D. Hawkes, "An overlap invariant entropy measure of 3D medical image alignment," *Pattern Recognition,* vol. 32, no. 1, pp. 71-86, 1999.

[13] M. Powell, "An efficient method for finding the minimum of a function of several variables without calculating derivatives," *Computer Journal,* vol. 7, no. 2, pp. 155-162, 1964.

[14] S. R. Yeratapally, C. Lang, A. Cerrone, G. Niebur and K. Cronberger, "Effect of defects on the constant-amplitude fatigue behavior of as-built Ti-6Al-4V alloy produced by laser powder bed fusion process: Assessing performance with metallographic analysis and micromechanical simulations," *Additive Manufacturing,* vol. 52, no. 102639, 2022.

[15] E. Gregory, E. Frankforter, P. Spaeth, W. Schneck and P. Juarez, "High Performance Simulation of Ultrasound Inspection of Porosity in Additively Manufactured Parts," *preprint,* 2023.

[16] L. Bauermann, L. Mesquita, C. Bischoff, M. Drews, O. Fitz, A. Heuer and D. and Biro, "Scanning acoustic microscopy as a non-destructive imaging tool to localize defects inside battery cells," *Journal of Power Sources Advances,* vol. 6, 2020.

[17] P. Virtanen and et.al., "SciPy 1.0: Fundamental Algorithms for Scientific Computing in Python," *Nature Methods,* vol. 17, no. 3, pp. 261-272, 2020.

[18] S. v. d. Walt, J. L. Schönberger, J. Nunez-Iglesias, F. Boulogne, J. D. Warner, N. Yager, E. Gouillart and T. Yu, "Sckit-image: image processing in Python," *PeerJ,* vol. 2, no. e453, 2014.

[19] F. Maes, A. Collignon, D. Vandermeulen, G. Marchal and P. Suetens, "Multimodality image registration by maximisation of mutual information," *IEEE Trans. Med. Images,* vol. 16, no. 2, pp. 187-198, 1997.